

ZENG, J., WANG, S., ZHANG, M., CAO, W., FERNANDEZ, C. and GUERRERO, J.M. 2024. Battery multi-time scale fractional-order modeling method for state of charge estimation adaptive to full parameters updating. *Journal of energy storage* [online], 86(part B), article number 111283. Available from: <https://doi.org/10.1016/j.est.2024.111283>

# Battery multi-time scale fractional-order modeling method for state of charge estimation adaptive to full parameters updating.

ZENG, J., WANG, S., ZHANG, M., CAO, W., FERNANDEZ, C. and GUERRERO, J.M.

2024

# Battery multi-time scale fractional-order modeling method for state of charge estimation adaptive to full parameters updating

Jiawei Zeng<sup>a,\*</sup>, Shunli Wang<sup>a,\*</sup>, Mengyun Zhang<sup>a</sup>, Wen Cao<sup>a</sup>, Carlos Fernandez<sup>b</sup>,  
Josep M. Guerrero<sup>c</sup>

<sup>a</sup> School of Information Engineering, Southwest University of Science and Technology, Mianyang 621010, China

<sup>b</sup> School of Pharmacy and Life Sciences, Robert Gordon University, Aberdeen AB10-7GJ, UK

<sup>c</sup> Department of Energy Technology, Aalborg University, Pontoppidanstraed, 1119220 Aalborg East, Denmark

\* Corresponding author.

E-mail address: wangshunli@swust.edu.cn (S. Wang).

## ABSTRACT

The fractional-order theory has been successfully applied to battery modeling and state of charge (SOC) estimation thanks to the rapid development of smart energy storage and electric vehicles. The fractional-order model (FOM) has high nonlinearity, which makes it difficult to identify the parameters of the FOM, especially the online identification of the order. Aiming at the problem of parameter identification and SOC estimation of the FOM of battery, a multi-time scale fractional-order modeling method is proposed in this paper. Then, a multi-time scale parameter identification strategy based on feature separation is proposed, and two sub-filters are used to complete the online identification of parameters. Finally, a fractional-order multi-innovation unscented Kalman filtering (FO-MI-UKF) algorithm is proposed for SOC estimation to utilize the value of historical information better. Under dynamic stress test (DST) and Beijing bus dynamic stress test conditions (BBDST), compared with the single-time scale parameter identification algorithm and the single-innovation SOC estimation algorithm, the root mean square error of the estimation results is reduced by 13.3 % and 8.7 %, respectively. The experimental results verify the effectiveness of the modeling method and provide a new idea for fractional-order modeling.

*Keywords:*

Lithium-ion batteries; Full parameter online identification; Fractional-order differential calculation; Modeling at multiple time scales; Battery state estimation

## 1. Introduction

### 1.1. Motivation and challenges

The increasingly severe energy shortage and environmental pollution are today's crises [1,2]. Lithium-ion batteries have attracted much attention because they can store renewable energy in nature and do not pollute [3–5]. Battery management system (BMS) can ensure the safe operation of the battery and effectively improve the performance of the battery by monitoring the state of the battery [6,7]. The high-precision battery model is the basis of state estimation [8]. The existing battery models mainly include electrochemical models [9,10], data-driven models [11–13], and equivalent circuit models [14–16]. The electro-chemical model considers the internal behavior of the battery, such as solid-liquid diffusion and charge transfer [9]. The detailed description of the internal mechanism gives the electrochemical model good voltage estimation performance, but the complex partial differential equation limits its application in electric vehicles. The data-driven model does not consider the internal mechanism, is divorced from the actual physical meaning, and requires a massive amount of high-quality training data [17]. In contrast, the equivalent circuit model has low computational complexity and can meet the accuracy requirements. In other words, it is necessary to build a high-fidelity battery model.

### 1.2. Literature review of battery modeling

The equivalent circuit model (ECM) can be divided into the integer-order model (IOM) and the FOM, which are composed of circuit elements with clear physical meaning, simple structure, and acceptable voltage estimation accuracy [14]. The second-order resistance-capacitance (RC) equivalent circuit model becomes the mainstream IOM because it integrates computational complexity and model accuracy [18]. Ref. [19] quantifies innovation based on time scale to realize the decoupling of complex dynamic behavior inside the battery and high-precision estimation of critical states. The IOM can be easily incorporated into the filter to estimate the SOC of the battery, and Ref [20] constructs an adaptive fault diagnosis framework based on multi-ECMs fusion, which can control the SOC estimation error within 1 %. In addition, the ECM is easy to implement for on-board applications, and Tian et al. [21] verified the effectiveness of ECM through hardware tests several years ago. However, due to its ideal electronic components, the IOM cannot accurately describe the nonlinear behavior inside the battery [22].

Given the highly nonlinear problem exhibited by the battery, researchers began to use Constant Phase Element (CPE) to replace the ideal capacitor [23–27], forming the FOM. Regarding model structure, CPE makes the voltage memory and non-uniformity, which can better fit the telephony impedance spectrum of the battery. Suppose there is a difference between the model structure and the actual characteristics of the battery. In that case, the perfect parameter identification algorithm will also lead to a loss of accuracy. Regarding model accuracy, existing studies have demonstrated that the voltage estimation error of the FOM is smaller than that of the IOM. Under the Federal Urban Driving Schedule (FUDS) and the United States 06

Cycle (US06) working conditions, the voltage estimation accuracy of FOM established by Chen et al. [28] is higher than that of the second-order RC model. Meanwhile, researchers applied the FOM to the SOC estimation of batteries. The process of SOC estimation is the process in which the model terminal voltage tracks the actual terminal voltage, and the open circuit voltage (OCV) and SOC functional relationship couple the two. The polarization voltage modeling of the battery directly affects the terminal voltage output of the model, so the high-precision battery model has better SOC estimation performance. Chai et al. [26] proposed an adaptive fractional-order volume Kalman filtering algorithm with initial value compensation and proved the superiority of the proposed method through experiments. Under the FUDS test, the mean absolute error (MAE) and root mean square error (RMSE) of SOC estimation results of the FOM established by Wu et al. [29] are 0.44 % and 0.54 %, respectively. In addition, FOM is widely used in state of health (SOH) prediction. Ref. [30] proposed a dual filtering algorithm based on FOM to estimate the SOC and SOH of batteries. FOM has proved superior to IOM in both voltage simulation and SOC estimation.

Challenges and opportunities coexist. The advantages of FOM originate from its nonlinearity and are also limited by it, such as the parameter identification problem of FOM. The model's parameters are affected by temperature, SOC, working conditions, and other factors. Online parameter identification can improve the accuracy of the model and state estimation algorithm. The FOM in the above studies identifies the order of the model by offline methods. For example, the model parameters are identified by the ant colony algorithm in Ref. [23], and the order of the model is identified by the particle swarm optimization algorithm in Ref. [25]. The difficulty of FOM parameter identification lies in identifying the order of CPE, which makes it difficult for FOM to update model parameters with working conditions like IOM. Aiming at the problem of low robustness caused by fixed parameters, Ref. [25] uses a new parameter identification method. Firstly, the order of the model is obtained by the offline identification, and then the model parameters are identified by the recursive least squares method. However, considering that the internal reactions of the battery are affected by factors such as input, aging, and temperature, the order of the FOM is not fixed [31–33]. For the order update problem of the FOM, Wang et al. [34] proposed a collaborative method of Beetle Antennae Search and Recursive Least Squares to identify the parameters of the FOM. However, Ref. [34] identifies the parameters of the FOM online with the order. However, the CPE is a device whose properties are capacitive and resistive, and its capacitance value interacts with the order. Suppose the two parameters of a CPE are identified separately. In that case, there must be a deviation between the result and the model itself. Therefore, it is necessary to identify parameters and orders simultaneously in the online parameter identification of FOM.

The FOM solves the problem of nonlinearity and memory of the ECM in battery modeling but does not consider the multi-time scale effect of internal charge carriers in the polarization process [35–37]. Specifically, the time constants corresponding to the transfer and diffusion impedance of the battery charge are different, and the battery model parameters have varying frequencies [19,38–40]. An accurate battery model is the premise of accurate SOC estimation. At the same time, the multi-time effect will accumulate over time and cause the loss of model accuracy. In Ref. [14], an efficient adaptive multi-time scale identification strategy was proposed to capture the processes of charge transfer, electric double layer, and diffusion inside the battery. In addition, the memory property of the FOM makes it have higher SOC estimation accuracy, and it will consider the influence of historical information in the SOC estimation. However, the influence of historical information only exists in estimating the model voltage, which causes the filter not to utilize the historical information when estimating the SOC thoroughly and does not conform to the model characteristics [41–43].

### *1.3. Ideas and contributions*

Considering the online parameter identification of FOM and the multi-time scale effect of the battery, a multi-time scale fractional-order modeling method is proposed in this paper, and historical information is effectively used to estimate the SOC of the battery. The main contributions of this paper are as follows:

(1) Based on the parameter consistency of CPE in FOM and considering the multi-time scale effect of battery, an online multi-time scale fractional-order model (MTS-FOM) was established.

(2) A multi-time scale parameter identification strategy based on feature separation is established, which causes the battery model parameters to have different change frequencies. It uses two sub-filters to complete the identification.

(3) A FO-MI-UKF SOC estimation algorithm is proposed, which fully uses historical information and unifies the memory length of the fractional-order operator with the novel information length, thus enhancing the coupling between SOC estimation and model.

### *1.4 Organization of this paper*

The structure of this paper is as follows: Section 2 introduces a multi-time scale fractional-order model, and a full-parameter online identification method based on feature separation is proposed. Section 3 is devoted to the implementation of the SOC estimation. Section 4 is devoted to the experimental analysis. Section 5 is a conclusion.

## **2. Multi-time scale fractional-order model**

### *2.1. Development of the multi-time scale fractional-order models*

The consistency between the model and the battery is the key to evaluating the model's performance, and it is also an essential factor affecting the state estimation. The order of FOM is not fixed, and its parameter variations have different characteristics. In summary, an MTS-FOM is established in this paper, as shown in Fig. 1.

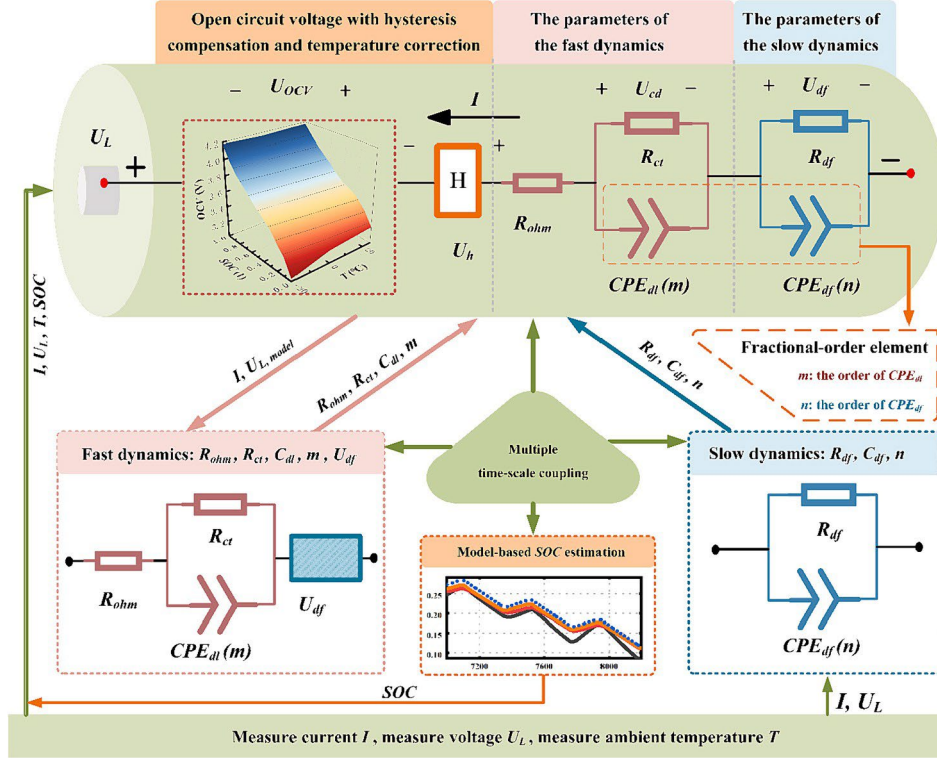


Fig. 1. Multi-time scale fractional-order modeling strategy for batteries

In Fig. 1,  $R_{ohm}$  represents the internal ohmic resistance,  $R_{ct}$  and  $R_{df}$  characterize internal charge transfer and diffusion resistances, respectively;  $U_{cd}$  and  $U_{df}$  are the voltages of the two polarization networks.  $CPE_{dl}$  and  $CPE_{df}$  are two CPEs with fractional-order characteristics.  $CPE_{dl}$  is a double-layer capacitance, which order is  $m$ .  $CPE_{df}$  is the diffusion capacitance, and its order is  $n$ . The fast dynamics represent the high-frequency fast dynamic response inside the battery, and the slow dynamics represent the low-frequency slow dynamic response inside the battery. The fast dynamic parameters are quite different from the slow dynamic parameters in the change frequency, so the model uses the amount of change in SOC as the discriminant condition. Specifically, the parameters in the fast dynamics are updated in response to SOC changes. In contrast, the parameters in the slow dynamics are updated after the amount of SOC change exceeds the set point. In addition, OCV is the battery's open circuit voltage, which considers the influence of temperature and hysteresis effects.  $U_h$  is the hysteresis voltage, and the value of  $U_h$  can be calculated in real-time using the current step function, as shown in Eq. (1).

$$U_{h,k} = \underbrace{\exp\left[\frac{-|\varepsilon T \eta I_{k-1}|}{Q_N}\right]}_{A_{h,k}} U_{h,k-1} + \underbrace{(1 - A_{h,k}) \text{sgn}(I_{k-1})}_{B_{h,k}} U_{H,k} \quad (1)$$

In Eq. (3),  $\varepsilon$  is a constant used to adjust the rate of decline,  $\eta$  is the Coulombic efficiency,  $U_H$  is the maximum hysteresis voltage,  $Q_N$  is the battery's nominal capacity,  $A_h$  is simplified form. The Grunwald-Letnikov (G-L) definition can simplify the derivative calculation and is more suitable for discrete systems [25]. This paper reduces the modeling complexity through the principle of short memory and only retains the historical information of a period [29], as shown in Eq. (2).

$$\begin{cases} d^{\alpha_k} x_k = \frac{1}{T^{\alpha_k}} \sum_{j=0}^L (-1)^j \binom{\alpha_k}{j} x_{k-j} \\ \binom{\alpha_k}{j} = \begin{cases} 1 & j=0 \\ \frac{\alpha_k(\alpha_k-1)\cdots[\alpha_k-(j-1)]}{j!} & j>0 \end{cases} \end{cases} \quad (2)$$

In Eq. (2),  $L$  is the memory length, and  $\alpha_k$  denotes the order of the system at time  $k$ . In general, the order  $\alpha$  is a constant value. The discretization expressions of  $U_{cd}$  and  $U_{df}$  can be obtained through the discretization definition of the G-L, as shown in Eq. (3).

$$\begin{cases} U_{cd,k} = \underbrace{\left(m_k - \frac{T^{m_k}}{R_{ct}C_{dl}}\right)}_{A_{cd}} \cdot U_{cd,k-1} + \underbrace{\frac{T^{m_k}}{C_{dl}}}_{B_{cd}} \cdot I_{k-1} - \underbrace{\sum_{j=2}^L (-1)^j \binom{m_k}{j}}_{F_{cd}} U_{cd,k-j} \\ U_{df,k} = \underbrace{\left(n_k - \frac{T^{n_k}}{R_{df}C_{df}}\right)}_{A_{df}} \cdot U_{df,k-1} + \underbrace{\frac{T^{n_k}}{C_{df}}}_{B_{df}} \cdot I_{k-1} - \underbrace{\sum_{j=2}^L (-1)^j \binom{n_k}{j}}_{F_{df}} U_{df,k-j} \end{cases} \quad (3)$$

In Eq. (3),  $A_{cd}$ ,  $A_{df}$ ,  $B_{cd}$ ,  $B_{df}$ ,  $F_{df}$ , and  $F_{cd}$  are concise representation,  $I_k$  is sampling current. In addition, the SOC of the battery is the predicted value, and its calculation is shown in Eq. (4).

$$S_k = S_{k-1} + (\eta/Q_N) \cdot I_{k-1} \quad (4)$$

In Eq. (4),  $S$  is the battery SOC. The  $U_{cd}$ ,  $U_{df}$ ,  $S$ , and  $U_h$  are taken as the model's state variables, and the model's state space expression equation is constructed as shown in Eq. (5).

$$\underbrace{\begin{bmatrix} U_{cd,k+1} \\ U_{df,k+1} \\ S_{k+1} \\ U_{h,k+1} \end{bmatrix}}_{x_{k+1}} = \underbrace{\begin{bmatrix} A_{cd} & 0 & 0 & 0 \\ 0 & A_{df} & 0 & 0 \\ 0 & 0 & 1 & 0 \\ 0 & 0 & 0 & A_{h,k} \end{bmatrix}}_{A_k} \underbrace{\begin{bmatrix} U_{cd,k} \\ U_{df,k} \\ S_k \\ U_{h,k} \end{bmatrix}}_{x_k} + \underbrace{\begin{bmatrix} B_{cd} & 0 \\ B_{df} & 0 \\ T \cdot \eta / Q_N & 0 \\ 0 & B_{h,k} \end{bmatrix}}_{B_k} \underbrace{\begin{bmatrix} I_k \\ U_{H,k} \end{bmatrix}}_{x_{k+1}} - \underbrace{\begin{bmatrix} \sum_{j=2}^L F_{cd} \cdot U_{cd,k-j} \\ \sum_{j=2}^L F_{df} \cdot U_{df,k-j} \\ 0 \\ 0 \end{bmatrix}}_{F_k} \quad (5)$$

Eq. (5) shows that the battery's state at a particular time is related to the historical information of a period, which reflects the memory characteristics of the battery. In addition, the hysteresis voltage is updated in real-time, enhancing the model's robustness. The terminal voltage output equation of the model is shown in Eq. (6).

$$U_{L,k} = U_{OC,k} + U_{h,k} - \underbrace{R_{ohm} I_k}_{U_{ohm}} - \underbrace{(U_{cd,k} + U_{df,k})}_{U_{CPE}} \quad (6)$$

## 2.2. Parameter identification mechanism based on feature separation

### 2.2.1. Cooperative estimation strategy for SOC and parameters

The internal reaction of the power lithium-ion battery includes particle diffusion and migration processes and shows different time-scale impedance characteristics [44]. The high-frequency behavior includes the pure resistive characteristics, electric double layer phenomenon, and charge transfer process. The specific model parameters include  $R_{ohm}$ ,  $R_{ct}$ ,  $C_{dl}$ , and  $m$ . The low-frequency manifestation is mainly the diffusion and mass transfer process of the reaction product in the active particle, and the specific model parameters include  $R_{df}$ ,  $C_{df}$ , and  $n$ . In summary, the high-frequency parameters of the model have small time constants and need to be updated at a faster frequency. Therefore, according to the different high and low-frequency characteristics, this paper proposes a parameter identification strategy based on feature separation, which can estimate SOC and identify model parameters simultaneously, as shown in Fig. 2.

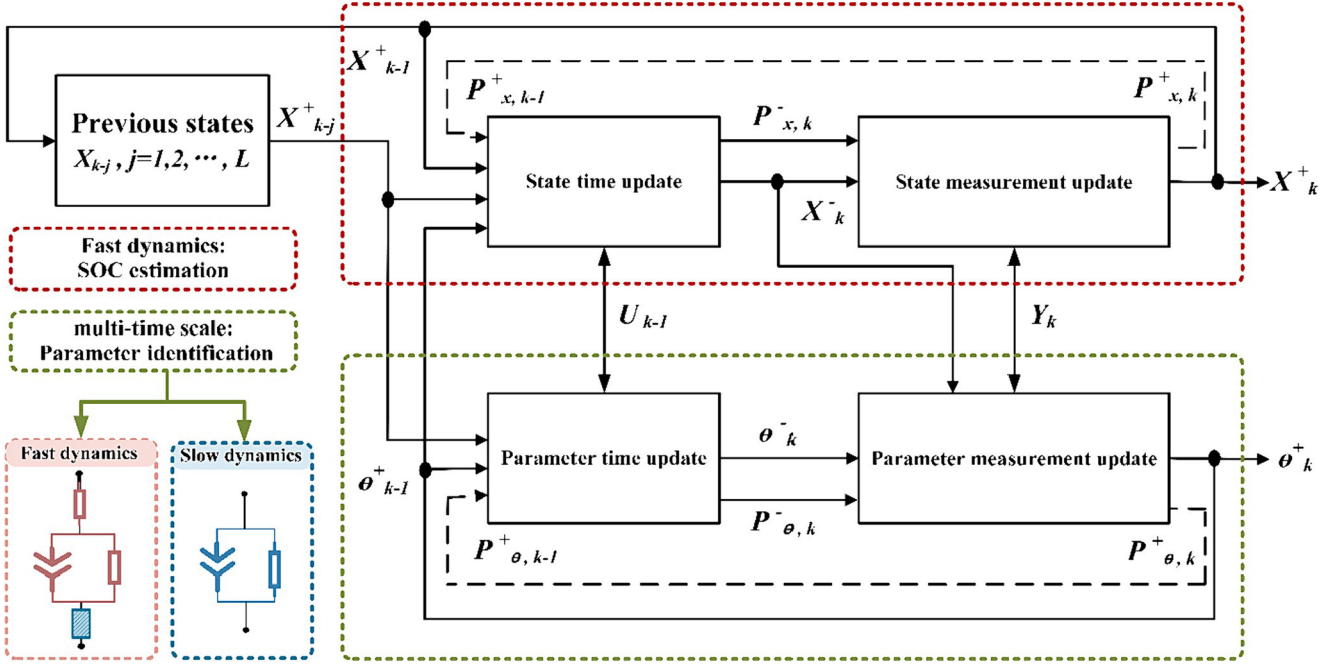


Fig. 2. A framework of parameter identification and state estimation based on feature separation.

It can be seen from Fig. 2 that two independent filters operate out of sync to estimate the battery SOC and model parameters, respectively. The parameter identification filter includes two extended Kalman filters with different time scales. The SOC requires high change frequency and filter accuracy, which belongs to fast dynamics, and its time scale is the sampling time. It is worth mentioning that the parameter identification filter transmits the latest parameter identification results to the state estimation filter for SOC estimation, which improves the estimation accuracy and robustness of SOC.

### 2.2.2. Fast dynamics parameters identification

The multi-time scale parameter identification strategy based on feature separation aims to improve the model's voltage accuracy and the battery's SOC estimation accuracy. The fast dynamics parameters of the model include  $R_{ohm}$ ,  $R_{ct}$ ,  $C_{dl}$ , and  $m$ . We can rewrite the output equation of the model, as shown in Eq. (7).

$$U_{L,k} = U_{OCV,k} + U_{h,k} - \underbrace{R_{ohm}I_k - U_{cd,k}}_{U_{fast}} - \underbrace{U_{df,k}}_{U_{slow}} \quad (7)$$

In Eq. (7),  $U_{OCV}$  is obtained by looking up the table of SOC and temperature, and  $U_h$  is calculated according to the current iteration. However, the parameters in fast dynamics are concentrated in  $U_{fast}$ , and the model's output cannot be calculated without knowing  $U_{df}$ . In this paper,  $U_{df}$  is regarded as a parameter to be identified in fast dynamics, and a high-frequency Kalman filtering is established. The state-space equation of fast dynamics is shown in Eq. (8).

$$\begin{cases} \theta_{fast,k+1} = \theta_{fast,k} + w_{fast,k}; \quad \theta_{fast} = [R_{ohm} \quad R_{ct} \quad C_{dl} \quad m \quad U_{df}]^T \\ \hat{U}_{L,k+1} = U_{OCV,k} + U_{h,k} - R_{ohm,k}I_k - \left( \left( m_k - \frac{T^{m_k}}{R_{ct,k}C_{dl,k}} \right) U_{cd,k-1} + \frac{T^{m_k}}{C_{dl,k}} I_{k-1} - \sum_{j=2}^L (-1)^j \binom{m_k}{j} U_{cd,k-j} \right) - U_{df,k} + v_{fast,k} \end{cases} \quad (8)$$

In Eq. (8),  $w_{fast}$  and  $v_{fast}$  represent observation noise and measurement noise, respectively.  $\theta_{fast}$  is the state variable, and  $\hat{U}_{L,k+1}$  is the estimated terminal voltage. To obtain the output matrix  $C_{fast}$  of the system, we define the relation shown in Eq. (9).

$$h_{fast}(x_k^+, I_k, \theta_{fast,k}) = U_{OCV,k} + U_{h,k} - R_{ohm,k}I_k - \left( \left( m_k - \frac{T^{m_k}}{R_{ct,k}C_{dl,k}} \right) U_{cd,k-1} + \frac{T^{m_k}}{C_{dl,k}} I_{k-1} - \sum_{j=2}^L (-1)^j \binom{m_k}{j} U_{cd,k-j} \right) \quad (9)$$

In Eq. (9),  $h_{fast}$  is a function of  $x^+$ ,  $I$ , and  $\theta_{fast}$ , and  $x^+$  denotes the posterior estimate of the model state. The difference between the model output and the measured terminal voltage is used as feedback correction. The calculation process of the output matrix  $C_{fast}$  is shown in Eq. (10).

$$C_{fast,k} = \left. \frac{\partial h_{fast}(x_k^+, I_k, \theta_{fast,k})}{\partial \theta_{fast}} \right|_{\theta_{fast} = \theta_{fast,k}^-} \quad (10)$$

$$\frac{\partial h_{fast}(x_k^+, I_k, \theta_{fast,k})}{\partial \theta_{fast}} = \frac{\partial h_{fast}(x_k^+, I_k, \theta_{fast,k})}{\partial R_{ohm}} + \frac{\partial h_{fast}(x_k^+, I_k, \theta_{fast,k})}{\partial R_{ct}} \frac{dx_k^-}{d\theta_{fast}}$$

In Eq. (10),  $\theta_{fast}$  represents a prior estimate of the fast dynamics parameter, and  $x^-$  represents a prior estimate of the model state. The detailed calculation process of the three parts in the second row of the equation is shown in Table 1.

**Table 1**

Details of the solution of the output matrix  $C_{fast}$ .

(1) The partial derivative of model output concerning fast dynamics parameters
$\frac{\partial h_{fast}(x_k^+, I_k, \theta_{fast,k})}{\partial \theta_{fast}} = \left[ \frac{\partial h_{fast}(x_k^+, I_k, \theta_{fast,k})}{\partial R_{ohm}} \quad \frac{\partial h_{fast}(x_k^+, I_k, \theta_{fast,k})}{\partial R_{ct}} \quad \frac{\partial h_{fast}(x_k^+, I_k, \theta_{fast,k})}{\partial CPE_{dl}} \quad \frac{\partial h_{fast}(x_k^+, I_k, \theta_{fast,k})}{\partial m} \quad \frac{\partial h_{fast}(x_k^+, I_k, \theta_{fast,k})}{\partial U_{df}} \right]$
$\frac{\partial h_{fast}(x_k^+, I_k, \theta_{fast,k})}{\partial U_{df}} = -1$
$\frac{\partial h_{fast}(x_k^+, I_k, \theta_{fast,k})}{\partial R_{ohm}} = -I_k$
$\frac{\partial h_{fast}(x_k^+, I_k, \theta_{fast,k})}{\partial R_{ct}} = -\frac{T^{m_k-1} x_k^+(1)}{R_{ct,k-1}^2 CPE_{dl,k-1}}$
$\frac{\partial h_{fast}(x_k^+, I_k, \theta_{fast,k})}{\partial CPE_{dl}} = -\frac{T^{m_k-1} x_k^+(1)}{R_{ct,k-1}^2 CPE_{dl,k-1}} + \frac{T^{m_k-1} I_k}{CPE_{dl,k-1}^2}$
$\frac{\partial h_{fast}(x_k^+, I_k, \theta_{fast,k})}{\partial m} = \frac{\ln(T) T^{m_k-1}}{R_{ct,k-1} CPE_{dl,k-1}} x_k^+(1) + \frac{\ln(T) T^{m_k-1}}{CPE_{dl,k-1}} I_k - x_k^+(1)$
(2) The partial derivatives of model outputs concerning model state variables
$\frac{\partial h_{fast}(x_k^+, I_k, \theta_{fast,k})}{\partial x_k^-} = \begin{bmatrix} -1 & -1 & \frac{dU_{OCV,k}}{dSOC} & 1 \end{bmatrix}$
(3) The partial derivatives of model state variables concerning fast dynamics parameters
$\frac{dx_k^-}{d\theta_{fast}} = \frac{\partial x_k^-}{\partial \theta_{fast}} + \frac{\partial x_{k-1}^-}{\partial x_{k-1}^+} \frac{dx_{k-1}^+}{d\theta_{fast}}$
The right-hand side of the equation is computed as follows:
$\frac{\partial x_k^-}{\partial \theta_{fast}} = \begin{bmatrix} 0 & \frac{\partial h_{fast}(x_k^+, I_k, \theta_{fast,k})}{\partial R_{ct}} & \frac{\partial h_{fast}(x_k^+, I_k, \theta_{fast,k})}{\partial CPE_{dl}} & \frac{\partial h_{fast}(x_k^+, I_k, \theta_{fast,k})}{\partial m} & & & \\ 0 & 0 & 0 & 0 & & & 1 \\ 0 & 0 & 0 & 0 & & & 0 \\ 0 & 0 & 0 & 0 & & & 0 \end{bmatrix}$
$\frac{\partial x_k^-}{\partial x_{k-1}^+} = A_{k-1}$
$\frac{dx_{k-1}^+}{d\theta_{fast}} = \frac{d[x_{k-1}^+ + K_{k-1}(U_{L,k-1} - \hat{U}_{L,k-1})]}{d\theta_{fast}} = \frac{dx_{k-1}^-}{d\theta_{fast}} - K_{k-1} \frac{d\hat{U}_{L,k-1}}{d\theta_{fast}} = \frac{dx_{k-1}^-}{d\theta_{fast}} - K_{k-1} \frac{\partial h_{fast}(x_{k-1}^+, I_{k-1}, \theta_{fast,k-1})}{\partial \theta_{fast}}$

In Table 1,  $A$  is the system matrix, and  $K$  is the gain. In the last formulation of Table 1, the decomposition of the posterior estimate to the prior estimate of the state variable is included. Therefore, in Table 1,  $K$  is the gain in the SOC estimation filter. There is an iterative computation logic in the computation of  $C_{fast}$ , which only needs to initialize  $\frac{dx_k^-}{d\theta_{fast}}$ ,  $\frac{\partial h_{fast}(x_k^+, I_k, \theta_{fast,k})}{\partial \theta_{fast}}$ , and  $\theta_{fast,k}$ . The high-frequency Kalman filtering is calculated as follows:

### Initialization:

Step 1: Initialization of parameters and error covariance matrix.

$$\hat{\theta}_{fast,0}^+ = E[\theta_{fast,0}]$$

$$P_{fast,0}^+ = E\left[\left(\theta_{fast,0} - \hat{\theta}_{fast,0}^+\right)\left(\theta_{fast,0} - \hat{\theta}_{fast,0}^+\right)^T\right] \quad (11)$$

### Prediction and correction:

Step 2: Predict the core temperature and external thermal resistance of the battery

$$\theta_{fast,k}^- = \theta_{fast,k-1}^+$$

$$P_{fast,k}^- = P_{fast,k-1}^- + P_{v_{fast}} \quad (12)$$

Step 3: Update the Kalman gain and calibrate the state variables

$$K_{fast,k} = P_{fast,k}^- \left( C_{fast,k} P_{fast,k}^- \left( C_{fast,k} \right)^T + P_{v_{fast}} \right)^{-1}$$

$$\hat{\theta}_{fast,k}^+ = \hat{\theta}_{fast,k}^- + K_{fast,k} (U_{L,k-1} - \hat{U}_{L,k+1}) \quad (13)$$

$$P_{fast,k}^+ = (E - K_{fast,k} C_{fast,k}) P_{fast,k}^-$$

In Eqs. (11)–(13),  $P_{fast}$  denotes the covariance matrix,  $E$  is the identity matrix, and  $K_{fast}$  is the Kalman gain. It is important to note that  $U_{df}$  is only a parameter in fast dynamics and does not consider the RC loop's internal relationships.

### 2.2.3. Slow dynamics parameters identification

The low-frequency performance is mainly the diffusion and mass transfer process of the reaction product in the active particle, and the specific model parameters include  $R_{df}$ ,  $C_{df}$ , and  $n$ . The slow dynamics parameters are contained in an RC link with no feedback correction mechanism. The  $U_{df}$  in fast dynamics parameters is updated at high frequency under measurement feedback with high confidence. Therefore, the identified  $U_{df}$  is taken as the measured value, and a slow dynamics filter is established. The feedback mechanism of  $U_{df}$  can enhance the coupling of model parameters at different time scales. The state space equation for the low-frequency RC link is shown in Eq. (14).

$$\begin{cases} \theta_{slow,k+1} = \theta_{slow,k} + w_{slow,k}; \theta_{slow} = [R_{df} \ C_{df} \ n]^T \\ \hat{U}_{df,k+1} = \left( n_k - \frac{T^{n_k}}{R_{df,k} C_{df,k}} \right) U_{df,k-1} + \frac{T^{n_k}}{C_{df,k}} I_{k-1} - \sum_{j=2}^L (-1)^j \binom{n_k}{j} U_{df,k-j} + v_{slow,k} \end{cases} \quad (14)$$

In Eq. (14),  $w_{slow}$  and  $v_{slow}$  represent observation noise and measurement noise, respectively.  $U_{df}$  is the voltage estimate of the low-frequency RC link. We further build the low-frequency Kalman filtering and define the relationship shown in Eq. (15).

$$h_{slow}(x_k^+, I_k, \theta_{slow,k}) = \left( n_k - \frac{T^{n_k}}{R_{df,k} C_{df,k}} \right) U_{df,k-1} + \frac{T^{n_k}}{C_{df,k}} I_{k-1} - \sum_{j=2}^L (-1)^j \binom{n_k}{j} U_{df,k-j} \quad (15)$$

The calculation process of output matrix  $C_{slow}$  for the slow dynamics system is shown in Eq. (16).

$$\begin{aligned} C_{slow,k} &= \left. \frac{\partial h_{slow}(x_k^+, I_k, \theta_{slow,k})}{\partial \theta_{slow}} \right|_{\theta_{slow} = \theta_{slow,k}^-} \\ \frac{\partial h_{slow}(x_k^+, I_k, \theta_{slow,k})}{\partial \theta_{slow}} &= \frac{\partial h_{slow}(x_k^+, I_k, \theta_{slow,k})}{\partial \theta_{slow}} + \frac{\partial h_{slow}(x_k^+, I_k, \theta_{slow,k})}{\partial x_k^-} \frac{dx_k^-}{\partial \theta_{slow}} \end{aligned} \quad (16)$$

In Eq. (16),  $\theta_{slow}^-$  represents a prior estimate of the slow dynamics parameter. The detailed calculation process of Eq. (16) is shown in Table 2.

**Table 2**

Details of the solution of the output matrix  $C_{slow}$

(1) The partial derivative of model output concerning slow dynamics parameters

$$\begin{aligned} \frac{\partial h_{slow}(x_k^+, I_k, \theta_{slow,k})}{\partial \theta_{slow}} &= \left[ \frac{\partial h_{slow}(x_k^+, I_k, \theta_{slow,k})}{\partial R_{df}} \quad \frac{\partial h_{slow}(x_k^+, I_k, \theta_{slow,k})}{\partial C_{df}} \quad \frac{\partial h_{slow}(x_k^+, I_k, \theta_{slow,k})}{\partial n} \right] \\ \frac{\partial h_{slow}(x_k^+, I_k, \theta_{slow,k})}{\partial R_{df}} &= -\frac{T^{n_k-1} x_k^+(2)}{R_{df,k-1}^2 CPE_{df,k-1}} \\ \frac{\partial h_{slow}(x_k^+, I_k, \theta_{slow,k})}{\partial C_{df}} &= -\frac{T^{n_k-1} x_k^+(1)}{R_{df,k-1}^2 CPE_{df,k-1}} + \frac{T^{n_k-1} I_k}{CPE_{df,k-1}^2} \\ \frac{\partial h_{slow}(x_k^+, I_k, \theta_{slow,k})}{\partial n} &= \frac{\ln(T) T^{n_k-1}}{R_{df,k-1} CPE_{df,k-1}} x_k^+(2) + \frac{\ln(T) T^{n_k-1}}{CPE_{df,k-1}} I_k - x_k^+(2) \end{aligned}$$

(2) The partial derivatives of model outputs concerning model state variables

$$\frac{\partial h_{slow}(x_k^+, I_k, \theta_{slow,k})}{\partial x_k^-} = [0 \ 1 \ 0 \ 0]$$

(3) The partial derivatives of model state variables concerning slow dynamics parameters

$$\frac{dx_k^-}{d\theta_{slow}} = \frac{dx_k^-}{\partial \theta_{slow}} + \frac{\partial x_k^-}{\partial x_{k-1}^+} \frac{dx_{k-1}^+}{d\theta_{slow}}$$

The right-hand side of the equation is computed as follows:

$$\frac{\partial x_k^-}{\partial \theta_{slow}} = \begin{bmatrix} 0 & 0 & 0 \\ \frac{\partial h_{slow}(x_k^+, I_k, \theta_{slow,k})}{\partial R_{df}} & \frac{\partial h_{slow}(x_k^+, I_k, \theta_{slow,k})}{\partial CPE_{df}} & \frac{\partial h_{slow}(x_k^+, I_k, \theta_{slow,k})}{\partial n} \\ 0 & 0 & 0 \\ 0 & 0 & 0 \end{bmatrix}$$

$$\frac{\partial x_k^-}{\partial x_{k-1}^+} = A_{k-1}$$

$$\frac{dx_{k-1}^+}{d\theta_{slow}} = \frac{d[x_{k-1}^- + K_{k-1}(U_{L,k-1} - \hat{U}_{L,k-1})]}{d\theta_{slow}} = \frac{dx_{k-1}^-}{d\theta_{slow}} - K_{k-1} \frac{d\hat{U}_{L,k-1}}{d\theta_{slow}} = \frac{dx_{k-1}^-}{d\theta_{slow}} - K_{k-1} \frac{\partial h_{slow}(x_{k-1}^+, I_{k-1}, \theta_{slow,k-1})}{\partial \theta_{slow}}$$

In Table 2, the iterative calculation process of the output matrix in the slow dynamics system is derived in detail. It is worth noting that the feedback mechanisms of slow dynamics systems differ from those of fast dynamics systems, but they both use the Kalman gain in SOC estimation. The parameter identification strategy based on different frequency domain characteristics is more consistent with the actual characteristics of the battery, and the model parameters can be updated adaptively in multi-time scales.

### 3. Model-based SOC estimation

#### 3.1. Fractional-order multi-innovation unscented Kalman filtering algorithm

For the highly nonlinear battery system, the processing method of the nonlinear problem will directly affect the SOC estimation accuracy. The unscented Kalman filtering (UKF) can solve the accuracy loss problem of the extended Kalman filtering (EKF) in solving the Jacobian matrix, and it is more suitable for battery system state estimation. In addition, the battery system has few observable variables, and the observation information should be fully utilized when estimating SOC.

The fractional-order systems can retain historical information, but the fractional-order unscented Kalman filtering (FOUKF) does not consider the impact of historical information during the state correction phase of the SOC. Specifically, the FOUKF will consider the state quantities from  $k-1$  to  $k-L$  when estimating the state at time  $k$ . However, the state correction process only considers the Kalman gain and innovation at time  $k$ . For this problem, this paper establishes the FO-MI-UKF algorithm for estimating the SOC of the battery. The state space expression of the model is given in Eq. (17).

$$\begin{cases} x_{k+1} = A_k x_k + B_k u_k - F_k + w_k \\ \hat{y}_k = h(x_k, u_k) + v_k = U_{OCV,k} + U_{h,k} - R_{ohm} I_k - U_{cd,k} - U_{df,k} + v_k \end{cases} \quad (17)$$

In Eq. (17),  $x$  is the system state variable,  $u$  is the system input, and  $A$  and  $B$  are the system matrix and input matrix, respectively.  $w$  is the system observation noise, and  $v$  is the system measurement noise. We extend a single innovation to a sequence of innovations, as shown in Eq. (18).

$$E_{L,k} = \begin{bmatrix} e_k \\ e_{k-1} \\ e_{k-2} \\ \vdots \\ e_{k-L+1} \end{bmatrix} = \begin{bmatrix} y_k - C_k \hat{x}_{k-} \\ y_{k-1} - C_{k-1} \hat{x}_{k-1-} \\ y_{k-2} - C_{k-2} \hat{x}_{k-2-} \\ \vdots \\ y_{k-L+1} - C_k \hat{x}_{k-L+1-} \end{bmatrix} \quad (18)$$

In Eq. (18),  $E_{L,k}$  is an innovation sequence with length  $L$ . In order to ensure the synchronous use of historical information, the length of innovation is set to the memory length of the fractional-order operator. Meanwhile, the single Kalman gain is extended to a Kalman gain sequence, as shown in Eq. (19).

$$K_{L,k} = [K_{1,k}, K_{2,k}, \dots, K_{L,k}] \in R^{n \times L} \quad (19)$$

In Eq. (19),  $K$  corresponds to the Kalman gain of the innovation at each time instant. Then, we can get the status update method of multiple innovations, as shown in Eq. (20).

$$\hat{x}_{k+}^+ = \hat{x}_{k-}^- + \sum_{i=1}^L F_{df,i} K_{i,k} e_{k-i+1} \quad (20)$$

In Eq. (20),  $F_{df}$  is the fractional-order attenuation weight coefficient in Eq. (5), which aims to reduce the weight of the old data. Specifically, the historical information close to the sampling moment has a higher weight. In summary, the detailed steps of the FO-MI-UKF algorithm are shown in Table 3.

**Table 3**

Detailed steps of the fractional-order multi-innovation unscented Kalman filtering.

**Step 1 Calculate the weight coefficient:**  $\lambda = a^2(n + \kappa) - n$ 

$$\begin{cases} W^{(m)}(0) = \frac{\lambda}{n + \lambda} \\ W^{(c)}(0) = W^{(m)}(0) + (1 - a^2 + b) \\ W^{(m)}(i) = W^{(c)}(i) = \frac{1}{2(n + \lambda)} \end{cases}$$

**Step 2 Initialize the state variables and error covariance matrix:**

$$\begin{cases} \hat{x}_0^+ = E[x_0] \\ P_0^+ = E((x_0 - \hat{x}_0^+)(x_0 - \hat{x}_0^+)^T) \end{cases}$$

**Step 3 Calculate the Sigma sampling point:**

$$\begin{aligned} \chi_0^- &= \hat{x}_{k-1}^+ \\ \chi_i^- &= \hat{x}_{k-1}^+ + \left( \sqrt{(n + \lambda)P_{k-1}^+} \right)_i, i = 1, \dots, n \\ \chi_i^- &= \hat{x}_{k-1}^+ - \left( \sqrt{(n + \lambda)P_{k-1}^+} \right)_i, i = n + 1, \dots, 2n \end{aligned}$$

**Step 4 Update the state process:**

$$\begin{aligned} d^\alpha \hat{x}_k^- &= \sum_{i=0}^{2n} (W_i^{(m)} f(\chi_i^-, u_{k-1})) \\ \hat{x}_k^- &= d^\alpha \hat{x}_k^- - \sum_{j=2}^L (F_{j,k-1} \hat{x}_{k-j}^+) \end{aligned}$$

**Step 5 Update the error covariance process:**

$$\begin{aligned} P_{xx} &= \sum_{i=0}^{2n} W_i^{(c)} (f(\chi_i^-, u_{k-1}) - d^\alpha \hat{x}_k^-) (f(\chi_i^-, u_{k-1}) - d^\alpha \hat{x}_k^-)^T + Q_{k-1} \\ P_{yx} &= \sum_{i=0}^{2n} W_i^{(c)} (\chi_i^- - \hat{x}_{k-1}^+) (f(\chi_i^-, u_{k-1}) - d^\alpha \hat{x}_k^-)^T \\ P_k^- &= P_{xx} + |F_{1,k-1}| P_{yx} + P_{yx} |F_{1,k-1}| + \sum_{j=2}^L (F_{j,k-1} P_{k-j}^+ F_{j,k-1}) + R_{k-1} \end{aligned}$$

**Step 6 Output the posteriori state estimate:**

$$\begin{aligned} \chi_i^+ &= f(\chi_i^-, u_{k-1}) - \sum_{j=2}^L (F_{j,k-1} \hat{x}_{k-j}^+) \\ \hat{y}_k &= \sum_{i=0}^{2n} (W_i^{(m)} h(\chi_i^+)) \end{aligned}$$

**Step 7 Update the state measurement:**

$$\begin{aligned} P_{yy} &= \sum_{i=0}^{2n} W_i^{(c)} (h(\chi_i^+) - \hat{y}_k) (h(\chi_i^+) - \hat{y}_k)^T; P_{xy} = \sum_{i=0}^{2n} W_i^{(c)} (\chi_i^+ - \hat{x}_k^-) (h(\chi_i^+) - \hat{y}_k)^T \\ K_k &= P_{xy} (P_{yy})^{-1}; \hat{x}_k^+ = \hat{x}_k^- + \sum_{i=1}^L F_{df,i} K_{i,k} e_{k-i+1} \end{aligned}$$

**Step 8 Update the error covariance matrix:**

$$P_k^+ = P_k^- + K_k P_{yy} K_k^T$$

**Step 9 The loop iteratively computes Step 3 to Step 8.**

In Step 1,  $a$  is the distribution parameter,  $n$  is the dimension of the state variable,  $\lambda$  is the adjustment coefficient, and  $b = 2$  for Gaussian distribution. The FO-MI-UKF algorithm can accurately estimate the SOC of the battery by cyclic iterative calculation.

### 3.2. Overall framework of modeling mechanism and estimation strategy

In general, after the establishment of the MTS-FOM, the fast dynamics parameters, including  $R_{ohm}$ ,  $R_{ct}$ ,  $C_{dl}$ ,  $m$ , and  $U_{df}$ , are identified by high-frequency Kalman filtering. In slow dynamics, the  $U_{df}$  of high-frequency estimation is used as feedback, and a low-frequency filter identifies the  $R_{df}$ ,  $C_{df}$ , and  $n$ . In addition, the Kalman gain of SOC estimation is used in the parameter identification process, and the high-frequency parameters and low-frequency parameters are coupled through  $U_{df}$ . Therefore, the whole parameter identification and SOC estimation process is strongly coupled. Fig. 3 shows the modeling and SOC estimation framework of this paper.

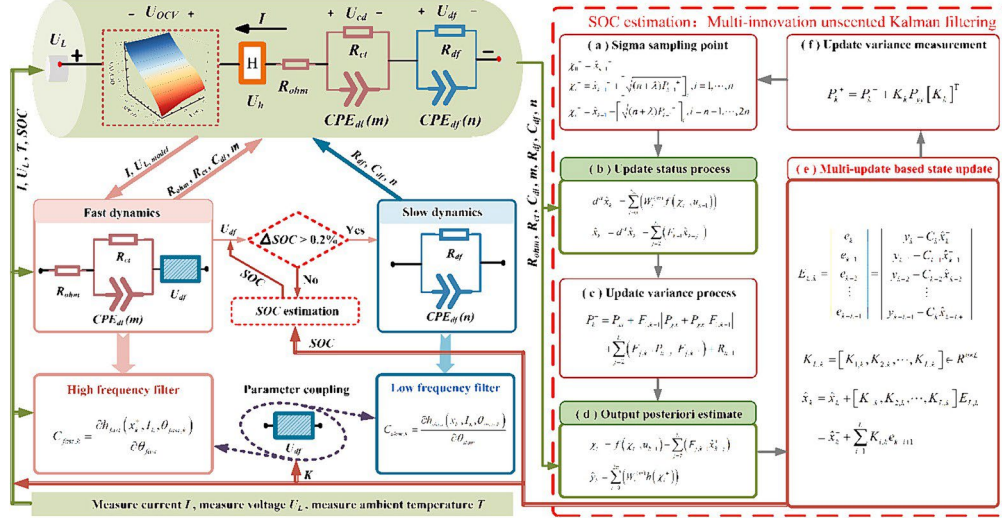


Fig. 3. Battery SOC estimation framework based on fractional-order multi-time scale modeling.

In Fig. 3, the Kalman gain in the FO-MI-UKF algorithm is used to identify the parameters of MTS-FOM, and the parameter identification results are used for SOC estimation. The multi-time scale parameter identification strategy based on feature separation is closer to the actual characteristics of the battery. In addition, due to the low-frequency update of some model parameters, the proposed method has lower computational complexity than the traditional single-time scale parameter identification method.

## 4. Experiments and result analysis

### 4.1. Experimental platform and design

An experimental test platform was built and tested to verify the performance of the proposed parameter identification strategy and SOC estimation algorithm under dynamic working conditions. The experimental testing platform includes a high-power charging-discharging tester, a central control computer, and a temperature control box. In addition, an unused ternary lithium-ion battery is selected as the test sample in this paper. Before the start of the test, the battery was charged to the cut-off voltage by constant current and constant voltage. The experimental test platform and battery information are shown in Fig. 4.

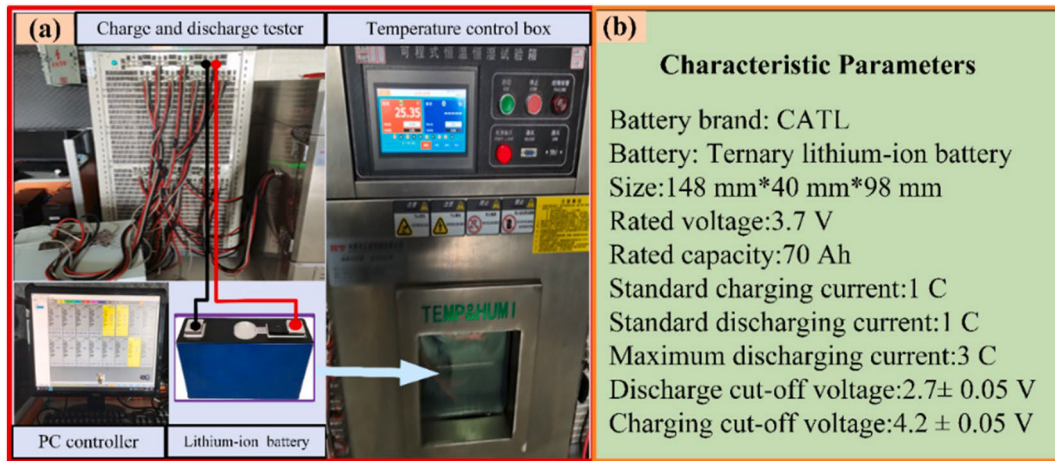


Fig. 4. (a): Experimental platform; (b) Characteristic battery parameters.

In Fig. 4, the temperature control box's temperature is 25 degrees Celsius. The experiments that were carried out include hybrid pulse power characterization (HPPC), DST, and BBDST. The terminal voltage accuracy of the model and SOC estimation accuracy of the battery were verified under different working conditions. The current and voltage under different working conditions are shown in Fig. 5.

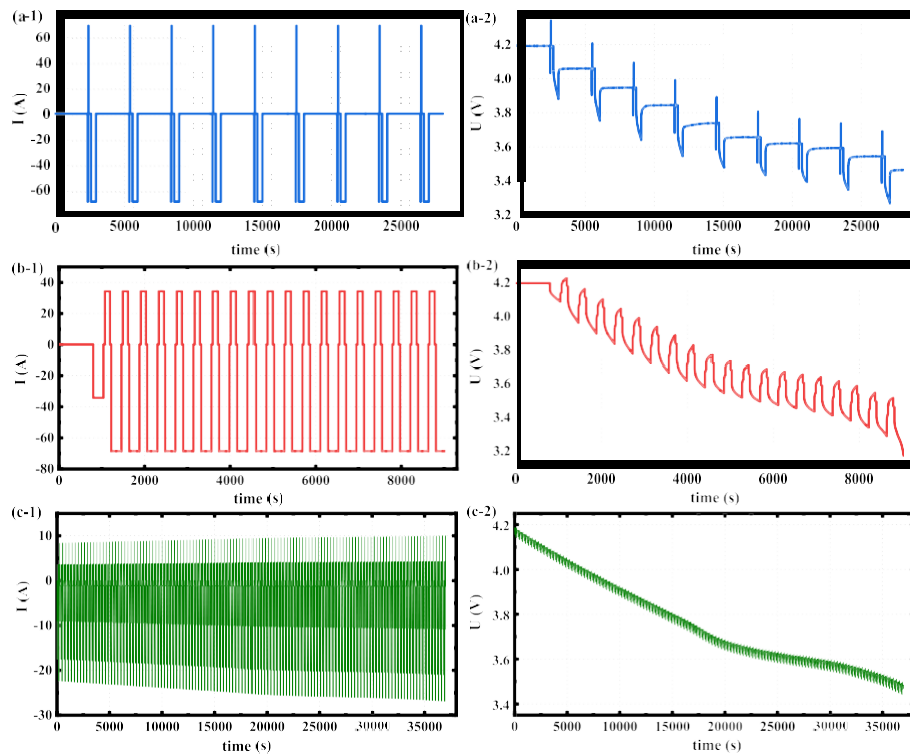


Fig. 5. Experimental results: (a-1) Current under HPPC; (a-2) Voltage under HPPC; (b-1) Current under DST; (b-2) Voltage under DST; (c-1) Current under BBDST; (c-2) Voltage under BBDST;

#### 4.2. Parameter identification results of the model

The parameters of the model, the accuracy of the model, and the SOC estimation accuracy of the battery interact with each other, so it is necessary to verify the identification effect of the model parameters. The initial values of the parameters are obtained by off-line identification using the genetic algorithm under different working conditions. The parameter identification results of MTS-FOM are shown in Fig. 6.

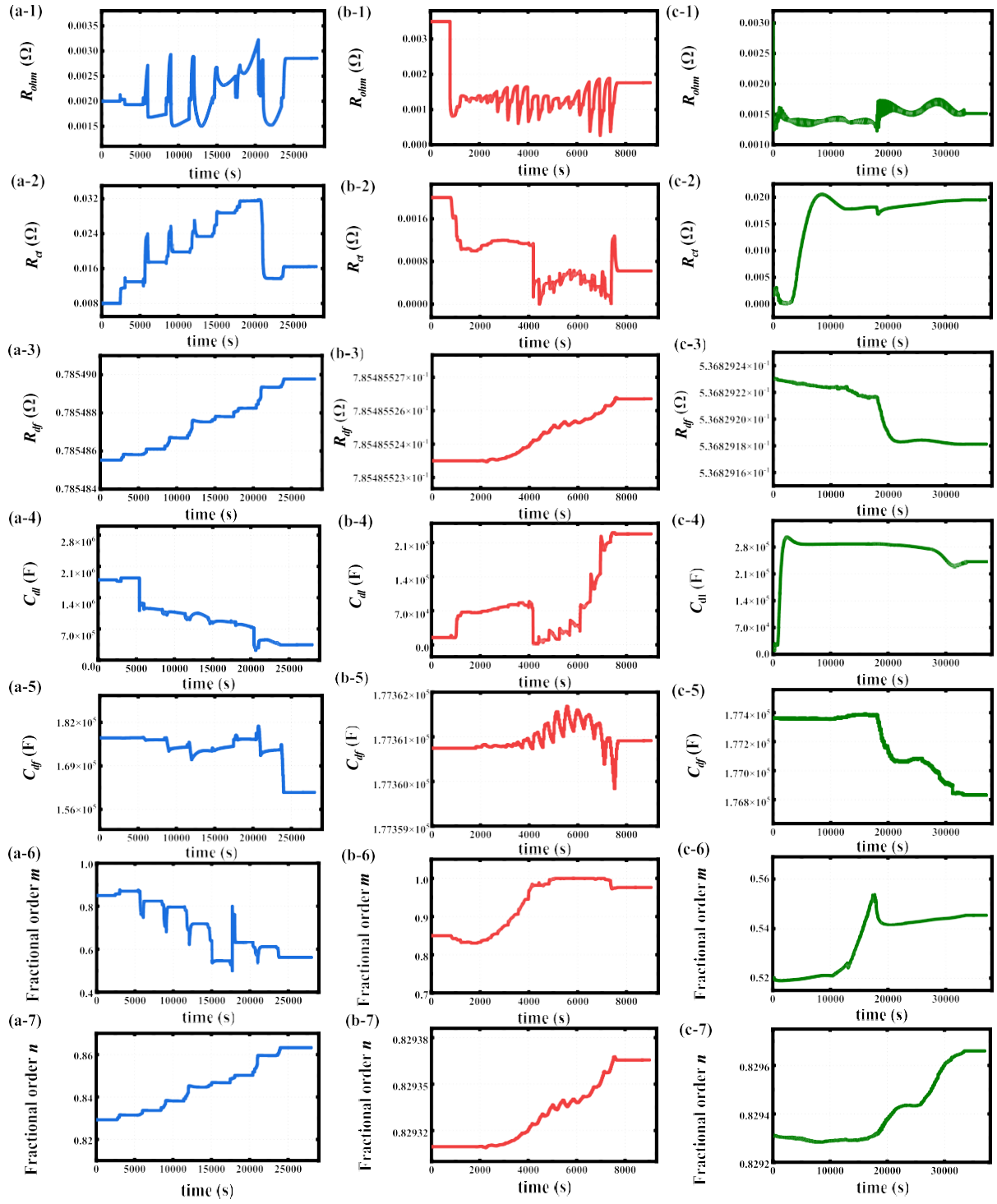
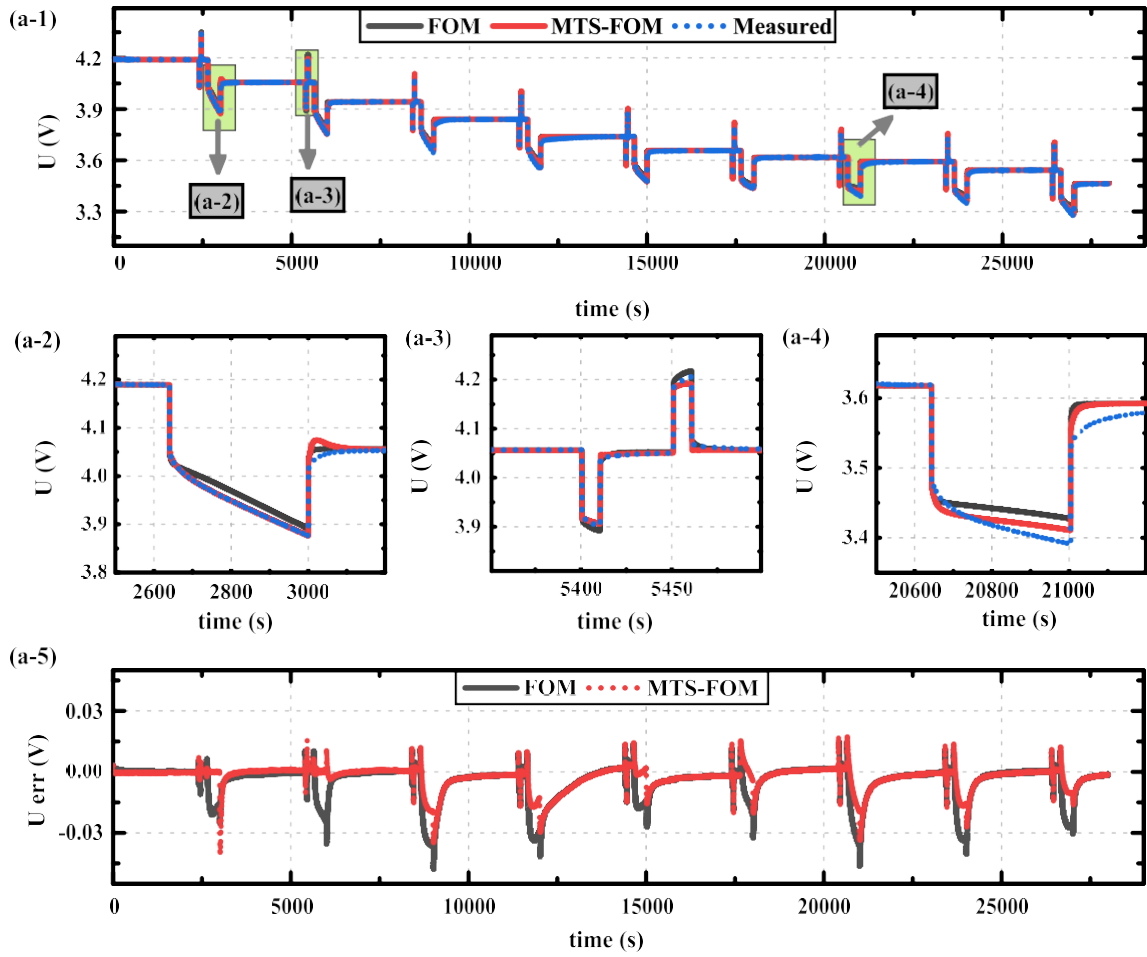


Fig. 6. Parameter identification results: (a) HPPC; (b) DST; (c) BBDST.

In Fig. 6, (a-1)-(a-7) is the identification result under HPPC, (b-1)-(b-7) is the identification result under DST, and (c-1)-(c-7) is the identification result under BBDST. It can be seen that the order of the model is not fixed in the test, and it will fluctuate in the SOC change. In addition, the time constant of the RC link is expressed as the product of capacitance and resistance. It can be seen that the time constant of the fast dynamics parameter is smaller than that of slow dynamics. An order of magnitude difference verifies the existence of a time scale difference between model parameters.

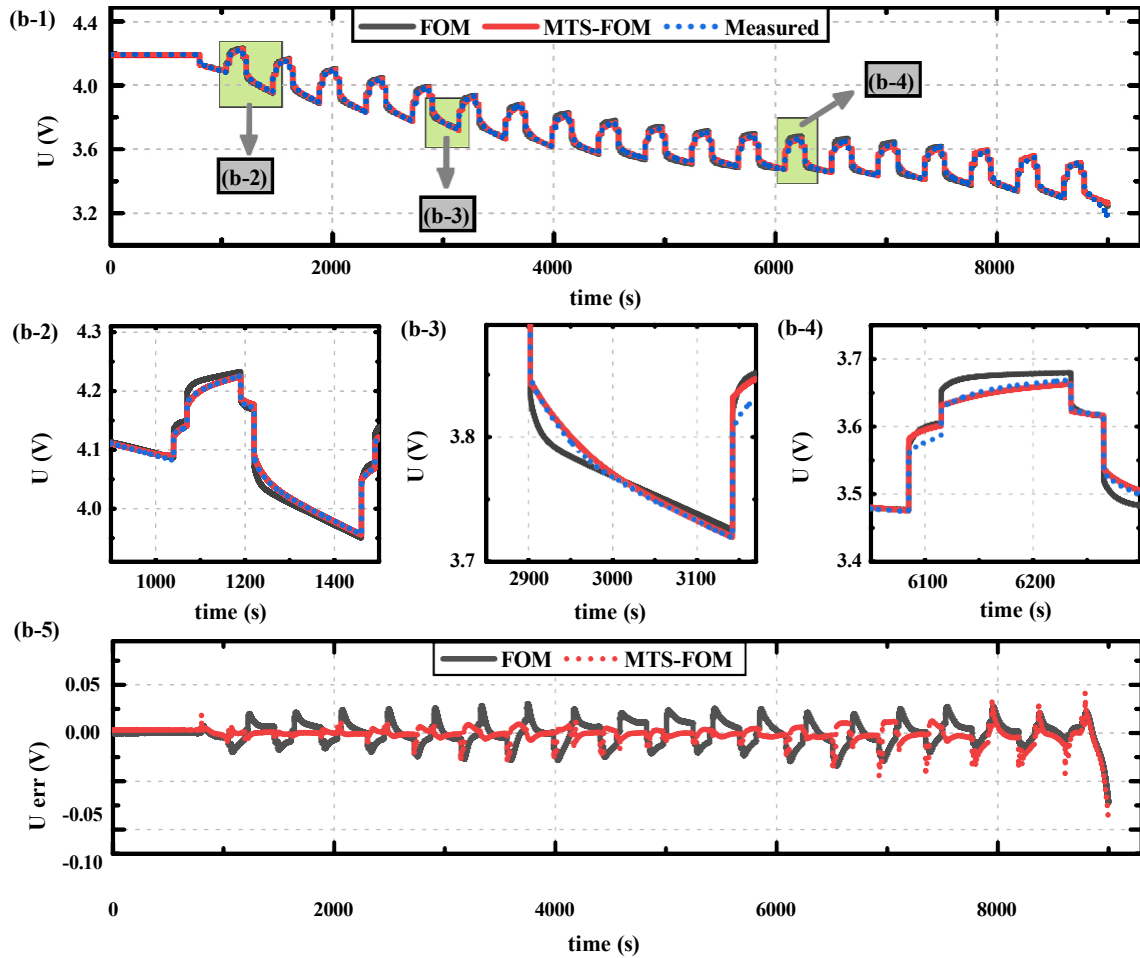
#### 4.3. Verification of terminal voltage tracking effect

The voltage estimation effect of the model can reflect the fit degree between the model and the battery, which is directly related to the SOC estimation accuracy. The terminal voltage values of batteries under different working conditions are taken as reference, and the estimation accuracy of the proposed model is compared with the traditional fractional order model (the EKF algorithm is used to identify parameters without considering the time scale effect). The estimated results of terminal voltage are shown in Fig. 7.



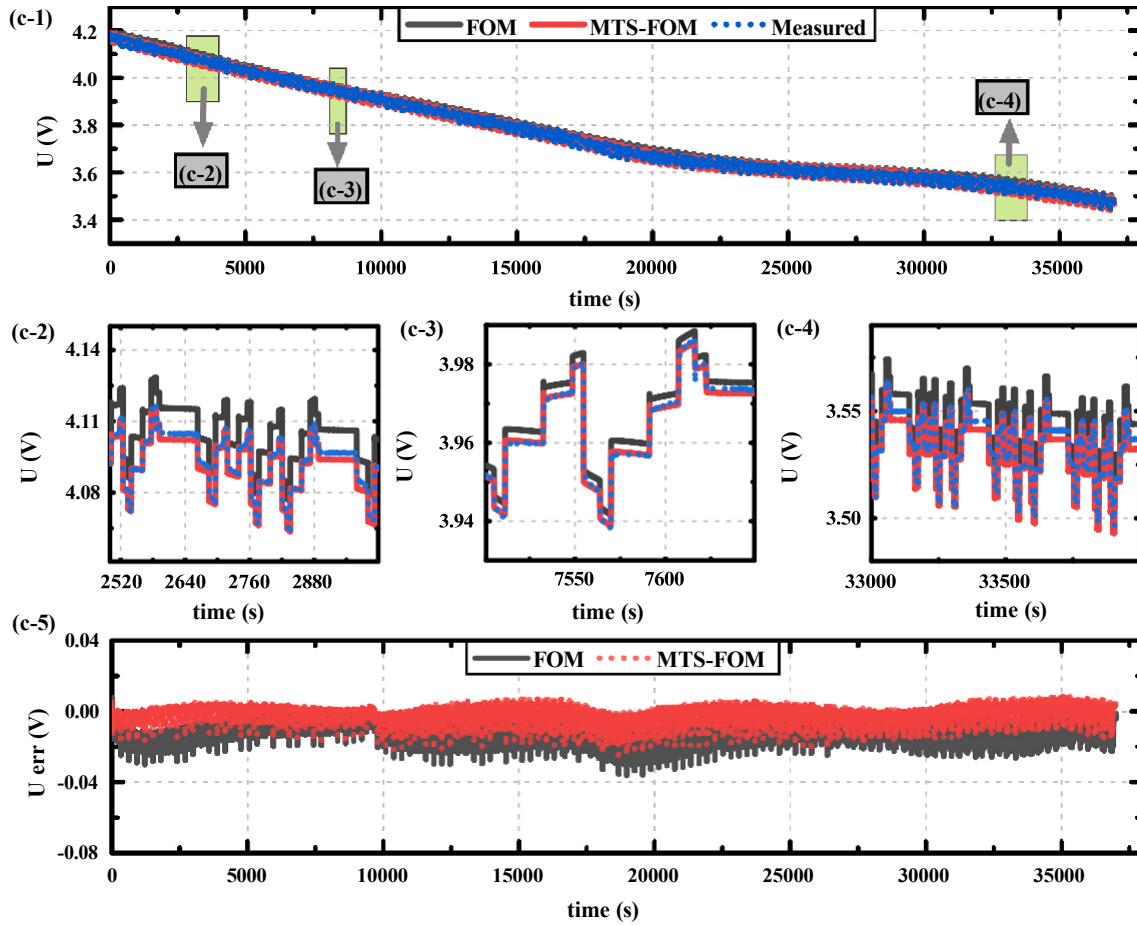
(a) Terminal voltage estimation results at HPPC

**Fig.7.** Terminal voltage estimation results: (a) HPPC; (b) DST; (c) BBDST.



(b) Terminal voltage estimation results at DST

Fig. 7. (continued).



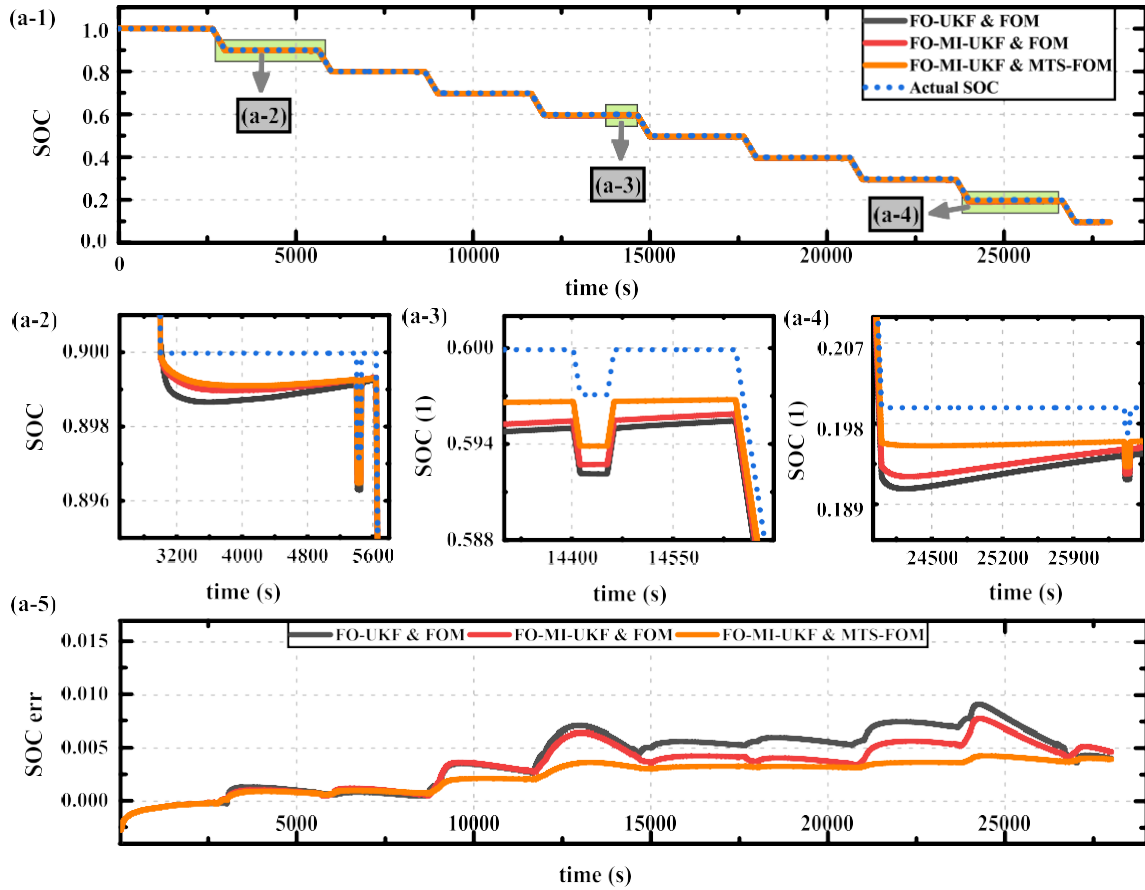
(c) Terminal voltage estimation results at BBDST

Fig. 7. (continued).

As seen in Fig. 7, both fractional-order models have good estimation accuracy of the terminal voltage. However, the MTS-FOM can better track the nonlinear change of battery voltage. It can be seen from Fig. 7 (b-3) that the MTS-FOM can accurately estimate the battery voltage at the beginning of the polarization behavior. At the same time, the FOM has significant errors in the polarization process. The MTS-FOM generally performs better voltage estimation under different working conditions, and its maximum error is less than 0.05 V.

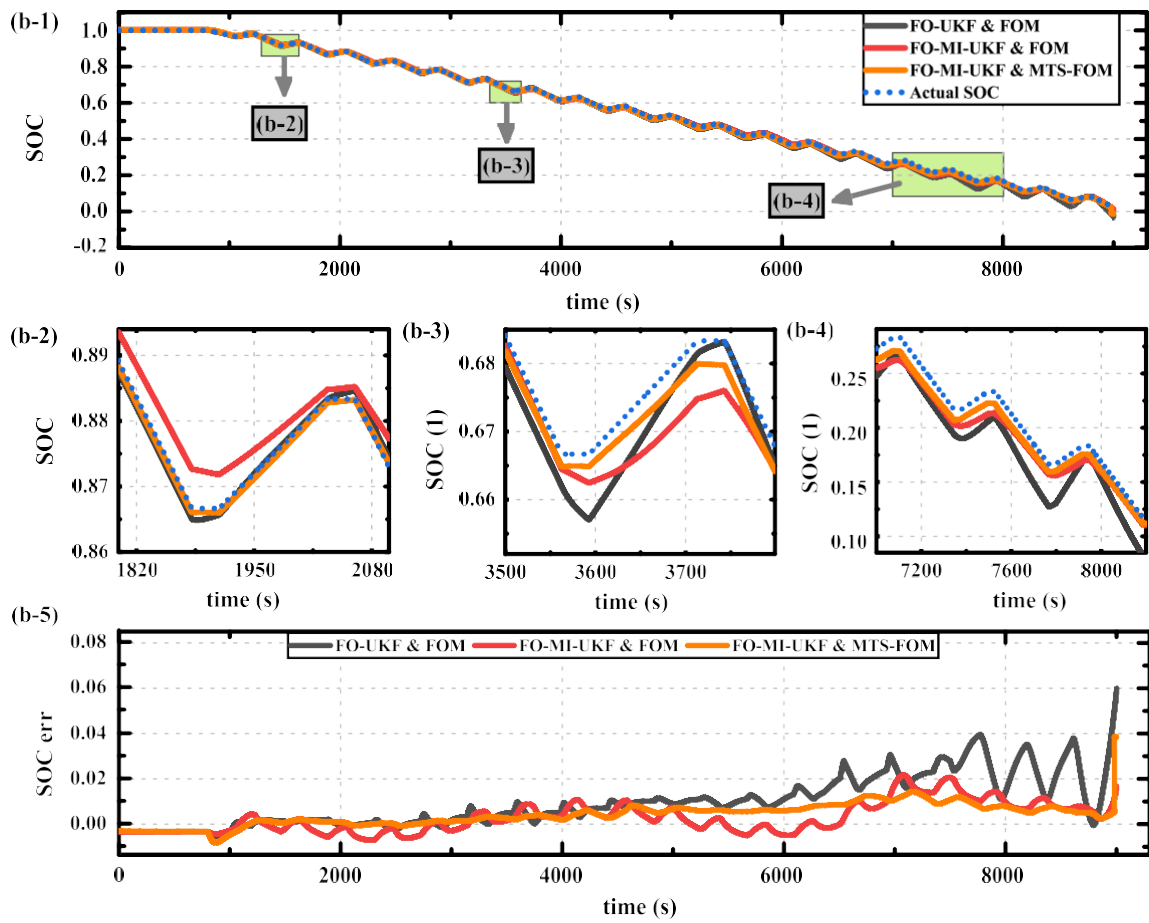
#### 4.4. Verification of SOC tracking effect

Based on MTS-FOM, the FO-MI-UKF algorithm, which is more suitable for fractional-order systems, is proposed in this paper. The current integral value in the experimental environment is used as the actual SOC, and the SOC estimation performance of different models and algorithms is compared. The battery test was carried out after full charge. The estimated SOC results under different working conditions are shown in Fig. 8.



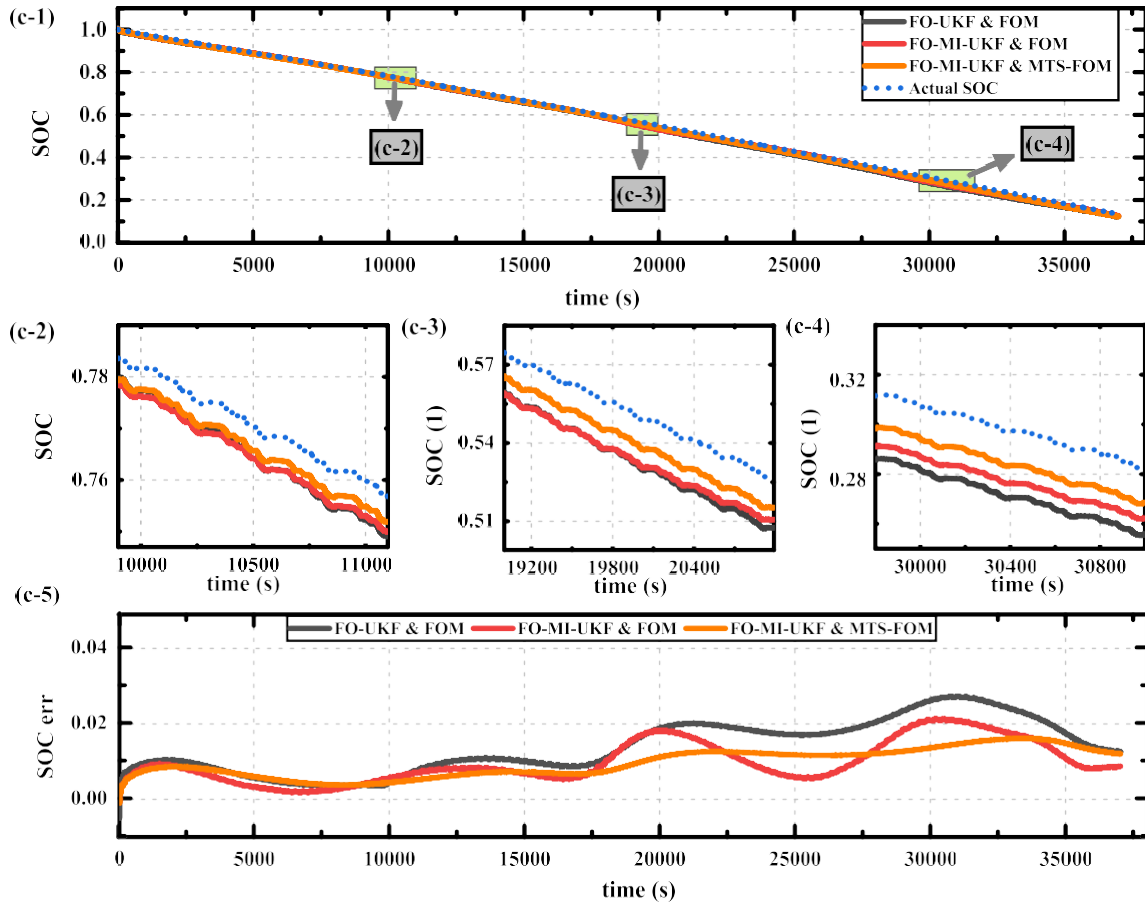
(a) SOC estimation results at HPPC

Fig. 8. SOC estimation results: (a) HPPC; (b) DST; (c) BBDST.



(b) SOC estimation results at DST

Fig. 8. (continued).



(c) SOC estimation results at BBDST

Fig. 8. (continued).

In Fig. 8, the FOM using the FO-MI-UKF algorithm has better SOC estimation performance; its error is maintained at about 1 %, and its RMSE under HPPC, DST, and BBDST working conditions are 0.0041, 0.0071, and 0.0110, respectively. The SOC estimation based on the FO-MI-UKF algorithm and the MTS-FOM has the best performance, which can accurately follow the SOC change under different working conditions. The RMSE under HPPC, DST, and BBDST working conditions are 0.0028, 0.0061, and 0.0101, respectively. The error analysis of the estimation results is shown in Fig. 9.

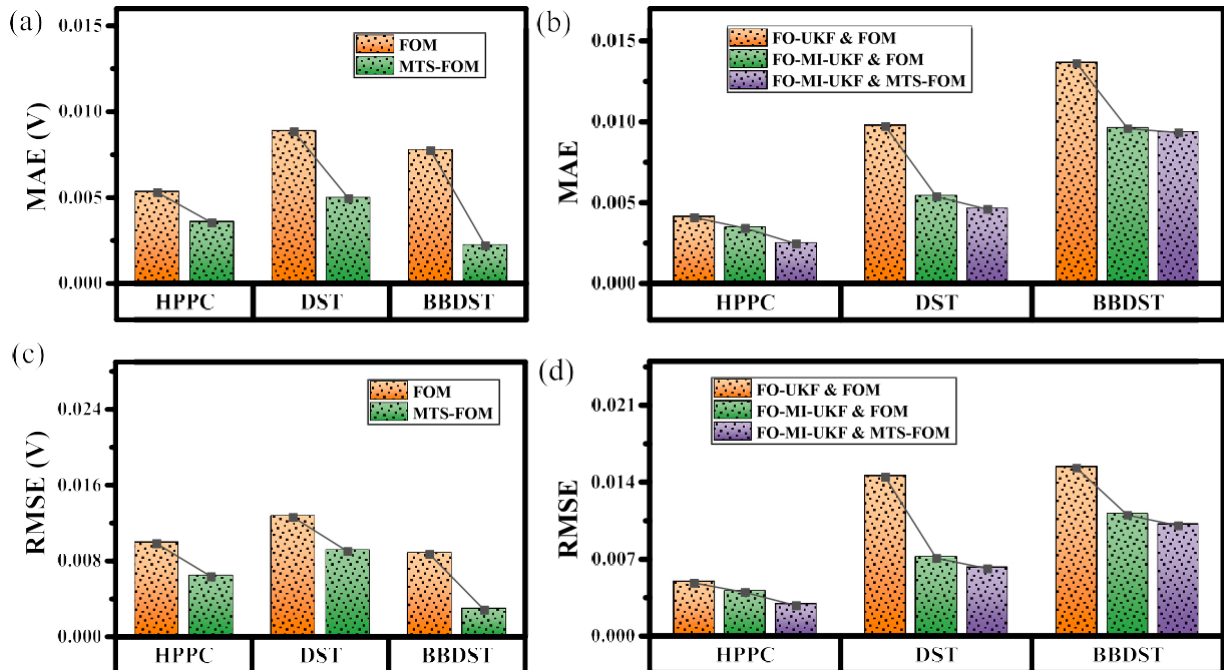


Fig. 9. Error analysis of the results: (a) MAE of the terminal voltage prediction error; (b) MAE of the SOC prediction error; (c) RMSE of the terminal voltage prediction error; (d) RMSE of the SOC prediction error.

**Fig. 9.** Error analysis of the results: (a) MAE of the terminal voltage prediction error; (b) MAE of the SOC prediction error; (c) RMSE of the terminal voltage prediction error; (d) RMSE of the SOC prediction error.

As shown in Fig. 9, the MTS-FOM based on feature separation has the best performance in estimating the terminal voltage and SOC of the battery. Meanwhile, the FO-MI-UKF algorithm integrating multi-innovation updates is more suitable for terminal voltage systems with memory characteristics. The comparison of other SOC estimation methods with the proposed method is shown in Table 4.

As seen from Table 4, among the existing SOC estimation methods, the method proposed in this paper has good estimation performance under the HPPC, DST, and BBDST working conditions.

**Table 4**  
Critical performance review of the proposed method with other existing SOC methods.

Methods	Battery	Verification	Error of SOC
Multi-model extended Kalman filtering (MM-EKF) [45]	Li-Ti battery 2.9 Ah	DST	RMSE: 0.52 %
FOM & Adaptive fractional-order cubature Kalman filtering (AFCKF) [26]	18650type lithium-ion battery 1.2 Ah	HPPC	RMSE: 2.74 %
FOM & Adaptive central difference Kalman filtering (ACDKF) [46]	NMC-based lithium-ion battery 94 Ah	DST New Europe Driving Cycle (NEDC)	RMSE(DST): 0.47 % RMSE (NEDC): 0.52 %
Positional encoded-attention long short-term memory (LSTM) [47]	A123 LiFePO4 battery 2.3 Ah	DST FUDS	RMSE(DST): 1.20 % RMSE (FUDS): 1.01 %
Proposed	Ternary lithium-ion battery 70 Ah	HPPC DST BBDST	RMSE (HPPC): 0.28 % RMSE(DST): 0.61 % RMSE (BBDST): 1.01 %

## 5. Conclusions

In this paper, the multi-time scale effect of the fractional-order model in parameter identification is studied, and the online parameter identification of the fractional-order model is realized by the method of feature separation. In addition, an fractional-order multi-innovation unscented Kalman filtering algorithm is proposed for the SOC estimation. The main conclusions are as follows.

- (1) The order of fractional-order model will change in application, and it has multi-time scale effect. The traditional single-time-scale fractional-order model results in the loss of precision in the process of parameter identification.
- (2) For the large-capacity commercial ternary lithium-ion battery used in this paper, the parameter identification strategy based on feature separation has higher voltage estimation performance in fractional-order modeling. And the accuracy is improved significantly in the case of continuous charging and discharging. The terminal voltage estimation results under the DST show that the RMSE of the multi-time scale fractional-order model is reduced by 28.6 %.
- (3) When using the fractional-order battery model to estimate SOC, the state update method of multi-innovation can improve the SOC estimation accuracy. The RMSE estimated of the SOC is reduced by 13.3 % and 8.7 % under DST and BBDST by fractional-order multi-innovation unscented Kalman filtering algorithm.

Although the proposed model has certain advantages, the multi-time scale fractional-order model needs to consider the effect of temperature on order, which is also our future research direction.

### CRedit authorship contribution statement

**Jiawei Zeng:** Writing – original draft, Project administration, Methodology, Data curation, Conceptualization. **Shunli Wang:** Writing –review & editing, Investigation, Funding acquisition. **Mengyun Zhang:** Software. **Wen Cao:** Resources, Project administration. **Carlos Fernandez:** Writing – review & editing, Visualization. **Josep M. Guerrero:** Writing – review & editing, Visualization, Validation.

### Declaration of competing interest

The authors declare that they have no known competing financial interests or personal relationships that could have appeared to influence the work reported in this paper.

## Data availability

Data will be made available on request.

## Acknowledgment

The work is supported by the National Natural Science Foundation of China (No. 62173281, 52377217, U23A20651) and the Sichuan Science and Technology Program (No. 24NSFSC0024, 23ZDYF0734, 2023NSFSC1436), Dazhou City School Cooperation Project (No. DZXQH006), Technopole Talent Summit Project (No. KJCRFH08), and Robert Gordon University.

## References

- [1] N. Zhang, et al., Review of heat pump integrated energy systems for future zero- emission vehicles, *Energy* 273 (2023).
- [2] S. Li, et al., Reliability assessment of renewable power systems considering thermally-induced incidents of large-scale battery energy storage, *IEEE Trans. Power Syst.* 38 (4) (2023) 3924–3938.
- [3] S.L. Wang, et al., An improved feedforward-long short-term memory modeling method for the whole-life-cycle state of charge prediction of lithium-ion batteries considering current-voltage-temperature variation, *Energy* 254 (2022).
- [4] D. Wang, Y. Yang, T. Gu, A hierarchical adaptive extended Kalman filter algorithm for lithium-ion battery state of charge estimation, *J. Energy Storage* (2023) 62.
- [5] B. Jiang, et al., An adaptive capacity estimation approach for lithium-ion battery using 10-min relaxation voltage within high state of charge range, *Energy* 263 (2023).
- [6] Y. Wang, et al., Perspectives and challenges for future lithium-ion battery control and management, *Etransportation* (2023) 18.
- [7] Y.-X. Wang, Z. Chen, W. Zhang, Lithium-ion battery state-of-charge estimation for small target sample sets using the improved GRU-based transfer learning, *Energy* 244 (2022).
- [8] X. Xiong, et al., State of health estimation for lithium-ion batteries using Gaussian process regression-based data reconstruction method during random charging process, *J. Energy Storage* (2023) 72.
- [9] Y. Wang, et al., An electrochemical-mechanical coupled multi-scale modeling method and full-field stress distribution of lithium-ion battery, *Appl. Energy* 347 (2023).
- [10] K. Jiang, et al., Study on evolution process and electrochemical behavior of porous cathode in discharge process of the solid-state lithium-oxygen battery, *J. Energy Storage* (2023) 74.
- [11] R. Xu, Y. Wang, Z. Chen, Data-driven battery aging mechanism analysis and degradation pathway prediction, *Batteries-Basel* 9 (2) (2023).
- [12] J. Xue, et al., Stacking integrated learning model via ELM and GRU with mixture correntropy loss for robust state of health estimation of lithium-ion batteries, *Energy* 284 (2023).
- [13] B. Jiang, et al., Mechanics-based state of charge estimation for lithium-ion pouch battery using deep learning technique, *Energy* 278 (2023).
- [14] X.Y. Yang, et al., Improved noise bias compensation-equivalent circuit modeling strategy for battery state of charge estimation adaptive to strong electromagnetic interference, *J. Energy Storage* (2023) 73.
- [15] H.T. Shi, et al., Improved multi-time scale lumped thermoelectric coupling modeling and parameter dispersion evaluation of lithium-ion batteries, *Appl. Energy* 324 (2022).
- [16] L. He, et al., An adaptive central difference Kalman filter approach for state of charge estimation by fractional order model of lithium-ion battery, *Energy* 244 (2022).
- [17] L. Zhou, et al., State estimation models of lithium-ion batteries for battery management system: status, challenges, and future trends, *Batteries-Basel* 9 (2) (2023).
- [18] E. Tian, et al., Security-ensured state of charge estimation of lithium-ion batteries subject to malicious attacks, *IEEE Transactions on Smart Grid* 14 (3) (2023) 2250–2261.
- [19] H. Shi, et al., Multi-time scale identification of key kinetic processes for lithium-ion batteries considering variable characteristic frequency, *J. Energy Chem.* 82 (2023) 521–536.
- [20] J. Li, et al., SOC estimation and fault diagnosis framework of battery based on multi-model fusion modeling, *J. Energy Storage* (2023) 65.
- [21] J. Tian, et al., Online simultaneous identification of parameters and order of a fractional order battery model, *J. Clean. Prod.* 247 (2020).
- [22] Y. Wang, M. Li, Z. Chen, Experimental study of fractional-order models for lithium-ion battery and ultra-capacitor: modeling, system identification, and validation, *Appl. Energy* 278 (2020).
- [23] X. Hu, et al., Co-estimation of state of charge and state of health for lithium-ion batteries based on fractional-order calculus, *IEEE Trans. Veh. Technol.* 67 (11) (2018) 10319–10329.
- [24] J. Zeng, et al., Improved fractional-order hysteresis-equivalent circuit modeling for the online adaptive high-precision state of charge prediction of urban-electric-bus lithium-ion batteries, *International Journal of Circuit Theory and Applications* 52 (1) (2023) 420–438.
- [25] L. Chen, et al., A novel combined estimation method for state of energy and predicted maximum available energy based on fractional-order modeling, *J. Energy Storage* (2023) 62.
- [26] H.Y. Chai, et al., State of charge estimation for lithium-ion batteries based on an adaptive fractional-order cubature Kalman filter with initial value compensation, *J. Energy Storage* (2023) 68.
- [27] R.H. Guo, W.X. Shen, Lithium-ion battery state of charge and state of power estimation based on a partial-adaptive fractional-order model in electric vehicles, *IEEE Trans. Ind. Electron.* 70 (10) (2023) 10123–10133.
- [28] L. Chen, et al., State-of-charge estimation of lithium-ion batteries based on fractional-order modeling and adaptive square-root cubature Kalman filter, *Energy* 271 (2023).
- [29] S.J. Wu, et al., A totally coupled multi time-scale framework containing full parameters online identification and SOC real-time estimation of lithium-ion battery based on a fractional order model, *J. Energy Storage* (2023) 73.
- [30] L.H. Ye, et al., Co-estimation of lithium-ion battery state-of-charge and state-of- health based on fractional-order model, *J. Energy Storage* (2023) 65.
- [31] B. Yang, et al., Offline order recognition for state estimation of Lithium-ion battery using fractional order model, *Appl. Energy* 341 (2023).
- [32] J. Antonio Lopez-Villanueva, et al., Application of variable-order fractional calculus to the modeling of calendar aging in Lithium-ion batteries, *Energies* 16 (5) (2023).
- [33] S. Mao, et al., Parameter identification method for the variable order fractional- order equivalent model of lithium-ion battery, *J. Energy Storage* (2023) 57.
- [34] J. Wang, et al., Identification of fractional-order equivalent circuit model of lithium-ion battery for improving estimation of state of charge, *J. Energy Storage* (2023) 70.
- [35] H. Shi, et al., On-line adaptive asynchronous parameter identification of lumped electrical characteristic model for vehicle lithium-ion battery considering multi- time scale effects, *J. Power Sources* 517 (2022).
- [36] X. Zhang, et al., A novel method for lithium-ion battery state of energy and state of power estimation based on multi-time-scale filter, *Appl. Energy* 216 (2018) 442–451.
- [37] H. Dai, et al., Adaptive model parameter identification for large capacity Li-ion batteries on separated time scales, *Appl. Energy* 184 (2016) 119–131.
- [38] J.-D. Gabano, T. Poinot, B. Huard, Bounded diffusion impedance characterization of battery electrodes using fractional modeling, *Commun. Nonlinear Sci. Numer. Simul.* 47 (2017) 164–177.
- [39] J. Song, M.Z. Bazant, Effects of nanoparticle geometry and size distribution on diffusion impedance of battery electrodes, *J. Electrochem. Soc.* 160 (1) (2013) A15–A24.
- [40] C. Qi, et al., On-line multi-time scale adaptive parameter identification based on improved lithium-ion batteries hysteresis characteristic-electrical equivalent circuit modeling, *J. Electrochem. Soc.* 170 (4) (2023).
- [41] J. Xu, D. Wang, A dual-rate sampled multiple innovation adaptive extended Kalman filter algorithm for state of charge estimation, *Int. J. Energy Res.* 46 (13) (2022) 18796–18808.
- [42] J. Wu, H. Xu, P. Zhu, State-of-charge and state-of-health joint estimation of lithium-ion battery based on iterative unscented Kalman particle filtering algorithm with fused Rauch-Tung-Striebel smoothing structure, *Journal of Electrochemical Energy Conversion and Storage* 20 (4) (2023).
- [43] M. Lei, et al., Double extended Kalman filter algorithm based on weighted multi- innovation and weighted maximum correlation entropy criterion for co-estimation of battery SOC and capacity, *ACS Omega* 8 (17) (2023) 15564–15585.
- [44] Y. Hu, Y.-Y. Wang, Asme, Real-time battery model identification using a two time- scaled approach, in: *ASME 2013 Dynamic Systems and Control Conference vol 3*, 2013.
- [45] H. Lv, et al., State of charge estimation of lithium-titanate battery based on multi- model extended Kalman filter considering temperature and current rate, *J. Energy Storage* (2024) 77.
- [46] L. He, et al., An adaptive central difference Kalman filter approach for state of charge estimation by fractional order model of lithium-ion battery, *Energy* 244 (2022).
- [47] S.A.A. Shah, et al., A novel positional encoded attention-based long short-term memory network for state of charge estimation of lithium-ion battery, *J. Power Sources* 590 (2024).